

Article

# The Facilitation of a Sustainable Power System: A Practice from Data-Driven Enhanced Boiler Control

Zhenlong Wu <sup>1</sup>, Ting He <sup>1</sup>, Li Sun <sup>2</sup> , Donghai Li <sup>1,\*</sup> and Yali Xue <sup>1</sup> 

<sup>1</sup> State Key Lab of Power Systems, Department of Energy and Power Engineering, Tsinghua University, Beijing 100084, China; WZLsongshanshan@163.com (Z.W.); he-t14@mails.tsinghua.edu.cn (T.H.); xueyali@tsinghua.edu.cn (Y.X.)

<sup>2</sup> Key Lab of Energy Thermal Conversion and Control of Ministry of Education, Southeast University, Nanjing 210096, China; sunli12@seu.edu.cn

\* Correspondence: lidongh@tsinghua.edu.cn

Received: 10 March 2018; Accepted: 4 April 2018; Published: 8 April 2018



**Abstract:** An increasing penetration of renewable energy may bring significant challenges to a power system due to its inherent intermittency. To achieve a sustainable future for renewable energy, a conventional power plant is required to be able to change its power output rapidly for a grid balance purpose. However, the rapid power change may result in the boiler operating in a dangerous manner. To this end, this paper aims to improve boiler control performance via a data-driven control strategy, namely Active Disturbance Rejection Control (ADRC). For practical implementation, a tuning method is developed for ADRC controller parameters to maximize its potential in controlling a boiler operating in different conditions. Based on a Monte Carlo simulation, a Probabilistic Robustness (PR) index is subsequently formulated to represent the controller's sensitivity to the varying conditions. The stability region of the ADRC controller is depicted to provide the search space in which the optimal group of parameters is searched for based on the PR index. Illustrative simulations are performed to verify the efficacy of the proposed method. Finally, the proposed method is experimentally applied to a boiler's secondary air control system successfully. The results of the field application show that the proposed ADRC based on PR can ensure the expected control performance even though it works in a wider range of operating conditions. The field application depicts a promising future for the ADRC controller as an alternative solution in the power industry to integrate more renewable energy into the power grid.

**Keywords:** Active Disturbance Rejection Control; Probabilistic Robustness; Monte Carlo; secondary air regulation

## 1. Introduction

In order to achieve sustainable energy development better and make full use of new energy, the use of renewable energy, such as solar, wind, and tidal power generation is expected to increase by 2.8% annually until the year 2040, and total renewable energy power generation will possess a share of one quarter of worldwide power by 2040 [1]. To integrate more renewable energy into the power grid, a growing requirement of load regulation is posed on conventional coal-fired units because of the intermittency of renewable energy. Now, more and more coal-fired units have to run in the load range of 50–100% and lift load frequently according to Automatic Generation Control (AGC) commands, which can be optimized by a modified differential evolution algorithm [2], and so on. Consequently, the dynamic characteristics of the control loops vary greatly, especially for those loops which are impacted by the load change, such as the superheated steam temperature loop, the main steam pressure loop, and the air loop. However, Proportional-Integral (PI) or Proportional-Integral-Derivative (PID) controllers

in coal-fired units cannot ensure a satisfactory control effect, which eliminates the error passively and is tuned in the nominal condition. The control design of coal-fired units is becoming a challenging task in view of the above-mentioned reasons.

To accommodate the uncertainties, two aspects in view of engineering practice should be considered. Firstly, the alternative solution should have a strong ability to deal with uncertainties, and should not rely on precise mathematical models. Some advanced control strategies, such as PI observer [3,4] and linear/nonlinear Internal Model Control (IMC) [5,6], have attracted many researchers' attention. The PI observer realizes disturbance estimations by the state observer, which has a similar structure to the Luenberger observer. IMC has a strong ability to deal with the model-plant mismatch and unmeasured disturbances [5]; however, it is hard to implement in a Distributed Control System (DCS) platform because of computation complexities. In this paper, a data-driven control strategy called Active Disturbance Rejection Control (ADRC) is utilized because of its ability to deal with uncertainties and its ease of use [7,8]. ADRC was originally proposed by Professor Han as a result of long-term thinking about model-based control theory and engineering control cybernetics [9]. Its core idea is that the internal uncertainties and external disturbances, called the total disturbance, are estimated in real time by an Extended State Observer (ESO) and compensated for by a feedback controller [10]. Linear ADRC is proposed to simplify parameter tuning and the design framework [11]. ADRC is distinctly different from other control strategies in the following respects: (i) it can estimate and compensate for total disturbance in real time and its structure is simple; (ii) ADRC can estimate the total disturbance by an ESO, which is unlike other observers, such as the Unknown Input Observer (UIO) and the Disturbance Observer (DOB) [12]; and (iii) ADRC is an energy-saving control and has less computation while the computational intensity of Model Predictive Control (MPC) is large and would result in additional hardware costs [13]. Because of the advantages mentioned above, ADRC has been applied in various areas, such as motion control systems [14], chemical process control systems [15], fuel cell systems [16], load frequency systems [17], Atomic Force Microscope (AFM) scanning systems [18], pressurized water reactor power [19] and fractional order systems [20]. Besides this, ADRC also has solved many benchmark problems successfully, such as the ALSTOM gasifier benchmark problem [21], the two-mass-spring benchmark problem [22], and the four tank benchmark problem [23]. Secondly, not only nominal plants but also plants which are far from being in a nominal condition should be considered in the process of parameter tuning. Most tuning methods of ADRC are proposed for the nominal model rather than those plants which are probably in a whole range of operating conditions [11,24]. Some other methods have been proposed only for particular plants, such as First Order Plus Time Delay plants (FOPTD) [25] and unstable processes [26]. Randomized algorithms are attracting more and more attention to analyze uncertain systems which could consider parameter uncertainties in the whole parameter space, including the "worst-case" condition [27–29]. Probabilistic Robustness (PR), as one of these randomized algorithms, is a practical and powerful tool to analyze uncertain systems and is utilized for controller tuning and robustness analysis [30]. So, PR is proposed to optimize the parameters of ADRC due to its practicability and the consideration of plants that are probably in a whole range of operating conditions.

The main contributions of this paper are as follows:

- (1) A data-driven boiler control method is proposed to increase the flexibility of the conventional power plant, thus being able to integrate more renewables into the grid.
- (2) An algorithm which is able to depict the stable region of ADRC is presented.
- (3) The proposed tuning method for ADRC is applied to the secondary air regulation of a boiler unit successfully.

The rest of the paper is organized as follows: the problem formulation, the calculation of the stability region, and PR-based ADRC tuning are depicted in Section 2. In Section 3, five simulations illustrate the effectiveness of the proposed method. Then, a field test of ADRC based on PR for the

secondary air regulation of a boiler unit was carried out and the effectiveness is proved. Finally, Section 5 offers concluding remarks.

## 2. Tuning of ADRC Based on PR

### 2.1. Problem Formulation

Parameter uncertainties, nonlinearity, and variation of dynamic characteristics caused by a wide range of operating conditions could be considered as parameter perturbation in a large space, so the problem formulation could be depicted as follows.

Considering a transfer function with parameter uncertainties in a parameter space  $Q$

$$G_p(s) = \frac{c_m s^m + c_{m-1} s^{m-1} + \dots + c_0}{a_n s^n + a_{n-1} s^{n-1} + \dots + a_0} e^{-\tau s} \quad (1)$$

where  $a_i (i = 0, 1, 2, \dots, n)$  and  $c_j (j = 0, 1, 2, \dots, m)$  are the coefficient of the denominator and the numerator, respectively. The order of the numerator is not greater than that of the denominator and the delay time  $\tau$  is a nonnegative real number. Due to the existence of parameter uncertainties, define  $\mathbf{q} = \{a_i, c_j, \tau\}$  as the random vector of parameter uncertainties throughout the parameter space  $Q$  according to the probability density function of  $p_r$ . The parameter space  $Q$  can be defined as:

$$Q = \left\{ [a_{i-}, a_{i+}] \cup [c_{j-}, c_{j+}] \cup [\tau_-, \tau+] \right\} \quad (2)$$

and the plant becomes a group of transfer functions.

The goal of control design is to meet design requirements in the whole parameter space, including the “worst-case” condition, that the design requirements may be the settling time, the integral of time and absolute error (ITAE), and overshoot.

The traditional tuning methods based on a nominal plant often have good control performance for the nominal plant. However, the control performance would be worse when the plant varies far from the nominal condition even though the controller is designed with robustness constraints and the simulations in Section 3 would emphasize this point. A seemingly good way is that controller tuning can go through any possible point in the parameter space  $Q$ , but it is impossible to be ergodic throughout the parameter space. The tuning method for ADRC based on PR could be a useful and highly efficient method which can consider probable plants.

### 2.2. The Fundamentals of ADRC

For ADRC design, a general nonlinear time-varying dynamic plant is assumed to have the following format:

$$y^{(n)}(t) = bu(t) + g\left(y^{(n-1)}(t), y^{(n-2)}(t), \dots, y(t), w(t)\right) \quad (3)$$

where  $y(t)$ ,  $u(t)$ ,  $w(t)$ , and  $b$  are the output, input, disturbance, and gain parameters of the plant, respectively.  $g$  is the synthesis of time-variance, disturbances, dynamic uncertainties, etc. of the plant. Define  $f = g\left(y^{(n-1)}(t), y^{(n-2)}(t), \dots, y(t), w(t)\right) + (b - b_0)u$  as a synthesis of the unknown dynamics, time-variant, nonlinear, and external disturbances of the plant, which is denoted the total disturbance and is assumed to be unknown in ADRC design. Plant (3) can be written as:

$$y^{(n)}(t) = b_0 u(t) + f\left(y^{(n-1)}(t), y^{(n-2)}(t), \dots, y(t), w(t)\right) \quad (4)$$

where  $b_0$  is the approximation of the gain parameter  $b$ .

The core idea of ADRC is to estimate the unknown total disturbance  $f$  by extending the total disturbance as an additional state. Assume that  $f$  is differentiable and  $\dot{f} = h$ . The plant in Equation (4) can be written as:

$$\begin{aligned} \dot{x} &= Ax + Bu + Eh \\ y &= C^T x \end{aligned} \quad (5)$$

where  $x = [x_1, x_2, \dots, x_n, x_{n+1}]^T = [y, \dot{y}, \dots, y^{(n)}, f]^T$ ,  $h = \dot{f}$ ,  $C^T = [1 \ 0 \ \dots \ 0]_{(n+1) \times (n+1)}$ , and

$$A = \begin{bmatrix} 0 & 1 & & \\ \vdots & & \ddots & \\ 0 & & & 1 \\ 0 & \dots & \dots & 0 \end{bmatrix}_{(n+1) \times (n+1)}, \quad B = \begin{bmatrix} 0 \\ \vdots \\ 0 \\ b \\ 0 \end{bmatrix}_{(n+1) \times 1}, \quad E = \begin{bmatrix} 0 \\ \vdots \\ 0 \\ 1 \end{bmatrix}_{(n+1) \times 1}.$$

The ESO for the plant in Equation (4) with  $y$  and  $u$  as inputs can be depicted as:

$$\begin{cases} \dot{z}_1 = z_2 + \beta_1(y - z_1) \\ \vdots \\ \dot{z}_{n-1} = z_n + \beta_{n-1}(y - z_1) \\ \dot{z}_n = z_{n+1} + \beta_n(y - z_1) + b_0 u \\ \dot{z}_{n+1} = \beta_{n+1}(y - z_1) \end{cases} \quad (6)$$

or

$$\dot{z} = A_e z + B_e y + C_e u \quad (7)$$

where  $z = \begin{bmatrix} z_1 \\ z_2 \\ \vdots \\ z_{n+1} \end{bmatrix}_{(n+1) \times 1}$ ,  $A_e = \begin{bmatrix} -\beta_1 & 1 & & \\ -\beta_2 & 0 & 1 & \\ \vdots & & \ddots & \ddots \\ -\beta_n & 0 & \dots & 0 & 1 \\ -\beta_{n+1} & 0 & \dots & 0 & 0 \end{bmatrix}_{(n+1) \times (n+1)}$ ,  $B_e = \begin{bmatrix} \beta_1 \\ \beta_2 \\ \vdots \\ \beta_{n+1} \end{bmatrix}_{(n+1) \times 1}$  and

$$C_e = \begin{bmatrix} 0 \\ \vdots \\ b_0 \\ 0 \end{bmatrix}_{(n+1) \times 1}.$$

$z_1, z_2, \dots, z_n$  aim at approximating  $y(t)$  and its derivatives (up to order  $n - 1$ ), and

$z_{n+1}$  can approximate the total disturbance  $f(t)$  when the observer gain vector  $B_e$  is tuned appropriately.

We can design the control law as follows:

$$u(t) = \frac{-z_{n+1}(t) + u_0(t)}{b_0} \quad (8)$$

where  $u_0(t)$  is to be determined afterward. The conventional plant (4) becomes:

$$y^{(n)}(t) = f - z_{n+1}(t) + u_0(t) \approx u_0(t) \quad (9)$$

then, the plant in Equation (4) can be seen as a cascaded integrators plant.

The final plant can be effectively controlled by using the following state-feedback law:

$$u_0(t) = k_1(r(t) - z_1(t)) + k_2(\dot{r}(t) - z_2(t)) + \dots + k_n(r^{(n-1)}(t) - z_n(t)) \quad (10)$$

where  $r(t)$  is the reference signal.

The final control law can be straightforwardly expressed as:

$$u(t) = \frac{k_1(r(t)-z_1(t))+k_2(\dot{r}(t)-z_2(t))+\dots+k_n(r^{(n-1)}(t)-z_n(t))}{b_0} - \frac{z_{n+1}(t)}{b_0} \tag{11}$$

$$=: K(\bar{r}(t) - z(t))$$

where  $\bar{r}(t) = [r(t)\dot{r}(t) \dots r^{(n-1)}(t) 0]^T$  and  $K = \frac{1}{b_0}[k_1 k_2 \dots k_n 1]_{1 \times (n+1)}$ , and  $K$  is the feedback gain vector.

As mentioned above, the structure of ADRC is shown in Figure 1 and ADRC can be expressed as the following state-space form:

$$\begin{cases} \dot{z}(t) = A_e z(t) + B_e y(t) + C_e u(t) \\ u(t) = K(\bar{r}(t) - z(t)) \end{cases} \tag{12}$$

where the parameters of ADRC are  $K$ ,  $B_e$ , and  $b_0$ . For simplifying tuning,  $K$  and  $B_e$  can be tuned based on the bandwidth-parameterization method as suggested in [11] and they can be determined by the controller bandwidth,  $\omega_c$ , and the observer bandwidth,  $\omega_o$ . The relationship of  $K$  and  $\omega_c$ ,  $B_e$ , and  $\omega_o$  can be shown as:

$$\begin{cases} k_i = \frac{n!}{(i-1)!(n+1-i)!} \omega_c^{n+1-i} & i = 1, 2, \dots, n \\ \beta_j = \frac{(n+1)!}{j!(n+1-j)!} \omega_o^j & j = 1, 2, \dots, n+1 \end{cases} \tag{13}$$

When  $n = 1$ , we can obtain  $k_1 = \omega_c$ ,  $\beta_1 = 2\omega_o$ , and  $\beta_2 = \omega_o^2$  for first-order ADRC.

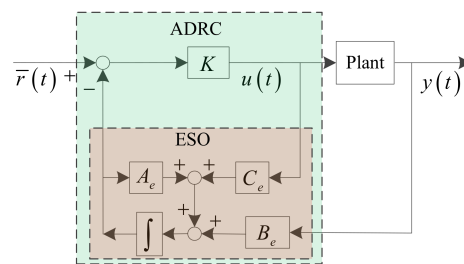


Figure 1. The structure of Active Disturbance Rejection Control (ADRC).

### 2.3. Stability Region of ADRC

It should be noted that ADRC has achieved a reasonable performance in spite of the order mismatch. First-order ADRC is widely used and is also the research focus in this paper.

In order to avoid the oscillation of the output, Equation (13) can be modified as follows:

$$\begin{cases} \beta_1 = 2\omega_o \\ \beta_2 = \zeta\omega_o^2 \end{cases} \tag{14}$$

where  $\zeta$  denotes a correction factor. The value of  $\zeta$  is often set in the range from 0.01 to 10 appropriately by lots of simulations.

An ADRC controller is equivalent to a 2 degree-of-freedom (TDOF) PID controller [31], here is the method for a first-order ADRC controller.

The ESO in Equation (6) for first-order ADRC can be rewritten in the form of transfer functions:

$$\begin{cases} z_1(s) = \frac{b_0 s}{s^2 + \beta_1 s + \beta_2} u(s) + \frac{\beta_1 s + \beta_2}{s^2 + \beta_1 s + \beta_2} y(s) \\ z_2(s) = \frac{-\beta_2 b_0}{s^2 + \beta_1 s + \beta_2} u(s) + \frac{\beta_2 s}{s^2 + \beta_1 s + \beta_2} y(s) \end{cases} \tag{15}$$

By applying Mason’s signal-flow gain formula, the structure of ADRC in Figure 1 can be transformed into an equivalent structure shown in Figure 2, and the specific derivations are omitted.

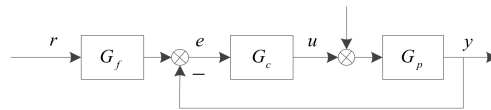


Figure 2. Equivalent structure of ADRC.

From Figure 2, the structure of ADRC is equivalent to a TDOF structure, where the feedback controller and the feedforward controller are:

$$G_c = \frac{(\xi\omega_0^2 + 2\omega_c\omega_0)s + \omega_c\xi\omega_0^2}{(s + 2\omega_0 + \omega_c)b_0s} \quad (16)$$

$$G_f = \frac{\omega_c(s^2 + 2\omega_0s + \xi\omega_0^2)}{(\xi\omega_0^2 + 2\omega_c\omega_0)s + \omega_c\xi\omega_0^2} \quad (17)$$

where the feedback controller  $G_c$  is equivalent to a PI controller plus a filter and the order of the numerator is bigger than that of the denominator for the feedforward controller.

It should be noted that ADRC can be formally equivalent to a TDOF structure, but it is still different from the traditional TDOF structure of a PID controller. Firstly, the feedback controller of the equivalent structure is a generalized PI controller plus a filter, which could avoid the occurrence of an ‘impulse spike’ in the controller’s output [32]. Secondly, the feedforward controller is different from the typical set-point weighing feedforward controller in the TDOF structure because of the order of  $G_f(s)$  [33]. Besides, to guarantee the stability of ESO, we should have  $\beta_1 > 0$  and  $\beta_2 > 0$ , implying  $\omega_o > 0$ . Otherwise, the ESO would be unstable [15].

Now, the D-partition method can be applied to analyze the stability region of the ADRC controller. To simplify the stability region analysis, the plant transfer function is represented as:

$$G_p(i\omega) = r(\omega)e^{i\theta(\omega)} = a(\omega) + ib(\omega) \quad (18)$$

and the characteristic equation for the closed-loop system is represented as [33]:

$$1 + G_p(s)G_c(s) = 0 \quad (19)$$

where  $G_l(s) = G_p(s)G_c(s)$  is called the open loop transfer function.

The boundaries of the stability region in the parameter plane consist of nonsingular boundaries for  $\omega \in (0, -\infty) \cup (0, +\infty)$  and singular boundaries for  $\omega = 0$  or  $\omega = \pm\infty$  based on the D-partition method.

The boundaries of the stability region can be determined as follows:

- (1) The singular boundary of ADRC for  $\omega = 0$  is (called  $\partial D_0$  surface)

$$\partial D_0 : \omega_c\xi\omega_0^2c_0 = 0 \quad (20)$$

Because we have  $\omega_o > 0$  and cannot always guarantee  $c_0 = 0$  for different plants, we can obtain that the singular boundary of ADRC is  $\partial D_0 : \omega_c = 0$ . Note that a pure time delay does not affect the singular boundary of ADRC ( $e^0 = 1$ ).

- (2) The singular boundaries of ADRC for  $\omega = \pm\infty$  are (called  $\partial D_\infty$  surface)

$$\partial D_\infty : b_0c_m = 0 \quad (21)$$

Considering that  $b_0$  is the approximation of the real gain, we can obtain that  $b_0 \neq 0$  and  $c_m = 0$  do not contain any parameter of ADRC, so we can neglect this singular boundary of ADRC.

(3) The nonsingular boundaries of ADRC for  $\omega \in (0, -\infty) \cup (0, +\infty)$  are (called  $\partial D_\omega$  surface)

$$\partial D_\omega : (\xi\omega_0^2 + 2\omega_c\omega_0) i\omega + \omega_c \xi \omega_0^2 (a(\omega) + ib(\omega)) + (i\omega + 2\omega_0 + \omega_c) b_0 i\omega = 0 \quad (22)$$

Separating the real and imaginary parts, we can obtain:

Above all, the stability region of first-order ADRC can be expressed as:

$$\partial D_\omega : \begin{cases} \omega_c (\xi\omega_0^2 - \omega^2) a(\omega) - (\xi\omega_0^2 + 2\omega_c\omega_0) b(\omega)\omega - \xi b_0 \omega^2 = 0 \\ \omega_c (\xi\omega_0^2 - \omega^2) b(\omega) + (\xi\omega_0^2 + 2\omega_c\omega_0) a(\omega)\omega + 2b_0 \omega_0 \omega = 0 \end{cases} \quad (23)$$

$$\begin{cases} \partial D_0 : \omega_c = 0 \\ \partial D_\omega : \begin{cases} \omega_c (\xi\omega_0^2 - \omega^2) a(\omega) - (\xi\omega_0^2 + 2\omega_c\omega_0) b(\omega)\omega - \xi b_0 \omega^2 = 0 \\ \omega_c (\xi\omega_0^2 - \omega^2) b(\omega) + (\xi\omega_0^2 + 2\omega_c\omega_0) a(\omega)\omega + 2b_0 \omega_0 \omega = 0 \end{cases} \\ \omega_0 > 0 \end{cases} \quad (24)$$

By solving Equation (24) with  $\omega$  varying from  $-\infty$  to  $+\infty$  when  $b_0$  and  $\xi$  are fixed, we obtain three curves which constitute the stability region of first-order ADRC.

#### 2.4. PR optimization

Define the parameters of an ADRC controller as  $d = \{\omega_c, b_0, \omega_0, \xi\}$ , which should be located in the stability region (22). When all of the uncertain plant and controller parameters are defined, the control system's performance can be evaluated by examining whether it satisfies the  $i$ th design requirements. For measuring design requirements on stability and performance quantitatively, a binary indicator function  $I$  is defined as follows

$$I_i = \begin{cases} 0 & \text{design requirements are not satisfied} \\ 1 & \text{design requirements are satisfied} \end{cases} \quad (25)$$

The probability  $P$  that the ADRC controller satisfies the design requirements can be described as the integral of the binary indicator function in the parameter space

$$P_i(d) = \int_Q I[G_p(q), G_c(d)] p_r(q) dq \quad (26)$$

By using this probabilistic framework, many control indices can be examined. Define the PR index as:

$$J(d) = fcn(P_1(d), P_2(d), \dots) \quad (27)$$

where  $fcn$  is defined as the weights for each index.

The goal of ADRC controller design is to find the optimal controller parameters  $d^*$  that obtain the maximum value of the index  $J(d^*)$  with the parameter uncertainties throughout the parameter space.

Considering that Equation (27) is difficult to integrate analytically in most cases, Monte Carlo simulation is a practical and useful tool to estimate the probability  $P$  [28]. The estimate of probability  $P$  and the PR index based on  $N$  samples

$$\hat{P}(d) = \frac{1}{N} \sum_{k=1}^N I[G_p(q), G_c(d)] \quad (28)$$

$$\hat{J}(d) = fcn(\hat{P}_1(d), \hat{P}_2(d), \dots) \quad (29)$$

and the estimate  $\hat{P}$  and  $\hat{J}$  approach to the real probability  $P$  and  $J$  in the condition of  $N \rightarrow \infty$ , respectively. However,  $N$  cannot tend to infinity in practice and a finite  $N$  results in estimation

errors. A minimum  $N$  which guarantees a certain confidence level to a risk parameter can be calculated based on the Massart Inequality [34,35]:

$$N > \frac{2(1 - \varepsilon + \frac{\alpha\varepsilon}{3})(1 - \frac{\alpha}{3}) \ln \frac{2}{\delta}}{\alpha^2\varepsilon} \quad (30)$$

where  $\varepsilon$  denotes the given risk parameter, the confidence level is defined as  $1 - \delta$ , and  $\alpha \in (0, 1)$ . Such a sample size ensures  $P_r\{|P_x - K/N| < \alpha\varepsilon\} > 1 - \delta$ , where  $P_x$  is the probability of the system to satisfy the design requirements,  $K/N$  is the estimated value of the probability,  $K$  is the number of design requirements satisfied in  $N$  samples, and the confidence interval is  $[K/N - \alpha\varepsilon K/N + \alpha\varepsilon]$ .

Considering the difficulty of non-convex problems for probability optimization [30], the genetic algorithm is proposed to optimize the controller parameters, which has a good global convergence ability and does not rely on any gradient or Hessian information [36].

Overall, the design procedure of an ADRC controller based on PR can be presented as:

- (1) Define control indices. The settling time and overshoot are the selected indices in this paper, and the weights are defined simultaneously.
- (2) The stability region  $D_c$  of the nominal plant is calculated according to Equation (24) as the search space of parameters.
- (3) Randomly generate parameters of the ADRC controller in region  $D_c$  as the initial population for the genetic algorithm. Calculate the probability function  $\hat{P}$  of the initial population as the object function for each set of parameters.
- (4) The genetic algorithm is applied to optimize parameters for finding the largest value of the object function  $\hat{P}$ . Define the optimized parameters as the expected parameters of the ADRC controller  $d'$ .
- (4) Test parameters  $d'$  by Monte Carlo simulation in the parameter space  $Q$ . If the result satisfies the requirement, the expected parameters are the optimal parameters  $d^*$ , otherwise return to step (3).

The estimated value of  $P$  can be fully close to the real value when  $N$  is big enough. To improve the calculation efficiency of genetic algorithms, a small value of  $N$  is set. A big enough value of  $N$  determined by the Massart Inequality according to risk parameter  $\varepsilon$  and the confidence level  $1 - \delta$  in Equation (30) can be used to test the probability of design requirements. Set the risk parameter  $\varepsilon = 0.1$ , the confidence level  $1 - \delta = 0.99$ , and  $\alpha = 0.2$  in this paper. Then, the minimum value of  $N$  for Monte Carlo simulation can be obtained as  $N = 2442$  according to the Massart Inequality.

### 3. Simulations

The proposed method is applied to five typical industrial plants, the first-order plus dead-time plant, the second-order plus dead-time plant, the non-minimum phase plant, the integral plant, and the high-order plant. The control performance is compared with the traditional TDOF PI controller based on PR and the IMC controller and PID controller tuned by an optimization algorithm with the Integral of Time and Absolute Error (ITAE) index for a nominal plant. The mathematical form of the feedforward controller and the feedback controller of the TDOF PI controller can be depicted as follows:

$$G_{f\_TDOF} = \frac{bk_p s + k_i}{k_p s + k_i} \quad (31)$$

$$G_{c\_TDOF} = k_p + \frac{k_i}{s} \quad (32)$$

where  $b$ ,  $k_p$ , and  $k_i$  are the parameters of the TDOF PI controller. The filter of the IMC controller is designed as:

$$G_{f\_IMC} = \frac{1}{T_{fs} + 1} \quad (33)$$

where  $T_f$  is the parameter of the filter and needs to be tuned. The mathematical form of the PID controller can be depicted as:

$$G_{PID} = k_{p1} + \frac{k_{i1}}{s} + k_{d1}s \tag{34}$$

where  $k_{p1}$ ,  $k_{i1}$ , and  $k_{d1}$  are the parameters of the PID controller and they are tuned with the ITAE index.

It should be noted that Padé approximations are applied to the TDOF PI controller’s design for  $G_1(s)$  and  $G_2(s)$  and the order of filters for the IMC controller is equal to the order of each plant. The necessary approximation is also applied to  $G_4(s)$  based on suitable all-pass characteristics [5]. Besides this, the PI controller for  $G_4(s)$  is a common PI controller because  $G_4(s)$  is an integral plant. The following simulations for  $G_4(s)$  are carried out with a PI controller rather than with a TDOF-PI controller.

The definitions of the PR index are varied based on design requirements, which can be a weight coefficient, a linear function, a nonlinear function, etc. Considering the conflicts between the settling time and overshoot, a linear function with a weighting coefficient is defined in this paper:

$$J(d) = 0.8P_{ts} + 0.2P_{\sigma} \tag{35}$$

where  $P_{ts}$ ,  $P_{\sigma}$  are the binary indicator functions of the system satisfying the design requirements of the settling time  $T_s$  and overshoot  $\sigma$ , respectively.

Note that the settling time  $T_s$  is the time required for the response curve to reach and stay within a range about the final value of the size specified by an absolute percentage of the final value (usually 2% or 5%, the former is chosen in this paper) and overshoot  $\sigma$  is the relative proportion between the difference and the steady state value where the difference is between the maximum peak value and the steady-state value. The number of individuals in the initial population and Monte Carlo simulation and the maximum number of evolutionary iterations are set to 200, 500, and 20, respectively.

The typical nominal plants and the parameter perturbation range of nominal plants are shown in Table 1. Besides this, the design requirements and parameters of the Massart Inequality for each plant are shown in Table 2.

**Table 1.** The typical plants and the parameter perturbation range.

Plant	The Nominal Model	Parameter Perturbation Range
$G_1(s) = \frac{1}{Ts + 1}e^{-\tau s}$	$T = 20, \tau = 200$	$T \in [10, 30], \tau \in [180, 220]$
$G_2(s) = \frac{1}{(T_1s + 1)(T_2s + 1)}e^{-\tau s}$	$T_1 = 20, T_2 = 20, \tau = 90$	$T_1 \in [16, 24], T_2 \in [16, 24]$ $\tau \in [80, 100]$
$G_3(s) = \frac{k(a - s)}{(T_1s + 1)(T_2s + 1)}$	$T_1 = 5, T_2 = 0.4, a = 1.25, k = 4$	$T_1 \in [4.5, 5.5], T_2 \in [0.36, 0.44]$ $a \in [1, 1.5], k \in [4.8, 3.2]$
$G_4(s) = \frac{k}{s(Ts + 1)}$	$T = 11, k = 0.2$	$T \in [7, 15], k \in [0.1, 0.3]$
$G_5(s) = \frac{k}{(Ts + 1)^3}$	$T = 5, k = 1.3$	$T \in [3, 7], k \in [1, 1.6]$

**Table 2.** Design requirements and parameters of Massart Inequality.

Plant	Design Requirements	Parameters of Massart Inequality
$G_1(s)$	$T_s < 1000s, \delta < 5\%$	$\epsilon = 0.01, \delta = 0.01, \alpha = 0.2, N = 24,495$
$G_2(s)$	$T_s < 700s, \delta < 5\%$	$\epsilon = 0.01, \delta = 0.01, \alpha = 0.2, N = 24,495$
$G_3(s)$	$T_s < 10s, \delta < 5\%$	$\epsilon = 0.1, \delta = 0.01, \alpha = 0.2, N = 2442$
$G_4(s)$	$T_s < 300s, \delta < 5\%$	$\epsilon = 0.01, \delta = 0.01, \alpha = 0.2, N = 24,495$
$G_5(s)$	$T_s < 240s, \delta < 5\%$	$\epsilon = 0.01, \delta = 0.01, \alpha = 0.2, N = 24,495$

Consider that  $b_0$  is the approximation of  $b$ ,  $b_0$  is fixed as 1 for plant 1, plant 2, plant 4, plant 5, and as 5 for plant 3, and there are three parameters  $k_p$ ,  $\omega_o$ , and  $\zeta$  to be tuned. Applying the proposed method, we can obtain the parameters of an ADRC controller based on PR. The parameters of the ADRC controller and other controllers are listed in Table 3.

Based on the parameters of the ADRC controller and contrasting controllers listed in Table 3, we can obtain step responses of these nominal plants in Table 1 with different controllers shown in Figure 3. A Monte Carlo simulation is also carried out  $N$  times, and the results are shown in Figures 4–8 with ITAE,  $T_s$ , and  $\sigma$ . Besides this,  $K/N$ , which is the estimated value of the probability, is listed in Table 4.

**Table 3.** The parameters of different controllers.

Plant	ADRC Controller	PID Controller	IMC Controller	TDOF-PI Controller
$G_1(s)$	$\omega_c = 0.2256,$ $\omega_o = 5.3506,$ $\zeta = 0.010$	$k_{p1} = 0.38,$ $k_{i1} = 0.0037,$ $k_{d1} = 12.88$	$T_f = 112.3$	$b = 0.6031,$ $k_p = 0.2509,$ $k_i = 0.0030$
$G_2(s)$	$\omega_c = 0.0314,$ $\omega_o = 2.9323,$ $\zeta = 0.0954$	$k_{p1} = 0.54,$ $k_{i1} = 0.0072,$ $k_{d1} = 14.22$	$T_f = 57.50$	$b = 0.4240,$ $k_p = 0.2661,$ $k_i = 0.0054$
$G_3(s)$	$\omega_c = 2.6275,$ $\omega_o = 3.3546,$ $\zeta = 0.1464$	$k_{p1} = 0.85,$ $k_{i1} = 0.11,$ $k_{d1} = 0.24$	$T_f = 0.965$	$b = 1.000,$ $k_p = 0.4245,$ $k_i = 0.0853$
$G_4(s)$	$\omega_c = 0.0192,$ $\omega_o = 0.1986,$ $\zeta = 2.6760$	$k_{p1} = 2.164,$ $k_{i1} = 0, k_{d1} = 9.233$	$T_f = 4.01$	$k_p = 0.1186, k_i = 0$
$G_5(s)$	$\omega_c = 0.3002,$ $\omega_o = 0.9273,$ $\zeta = 0.1529$	$k_{p1} = 0.346,$ $k_{i1} = 0.0384,$ $k_{d1} = 2.6507$	$T_f = 17.15$	$b = 0.9300,$ $k_p = 0.1877,$ $k_i = 0.0191$

PID = Proportional-Integral-Derivative; IMC = internal model control; TDOF-PI = 2 degrees of freedom proportional-integral.

**Table 4.** The estimated value of the probability.

Plant	ADRC Controller	PID Controller	IMC	TDOF-PI Controller
$G_1(s)$	0.9991	0.6487	0.9990	0.9989
$G_2(s)$	0.9991	0.8972	0.9992	0.9999
$G_3(s)$	0.9630	0.7732	0.9390	0.9523
$G_4(s)$	0.9999	0.8773	0.8385	0.9984
$G_5(s)$	1	0.8355	0.9844	0.9920

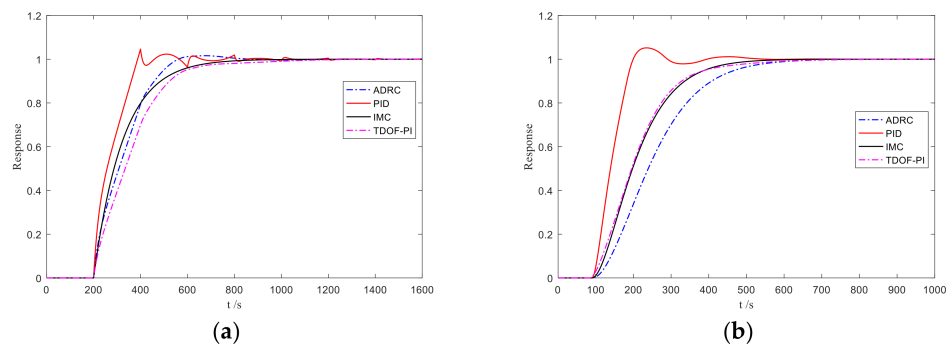


**Figure 3.** Cont.

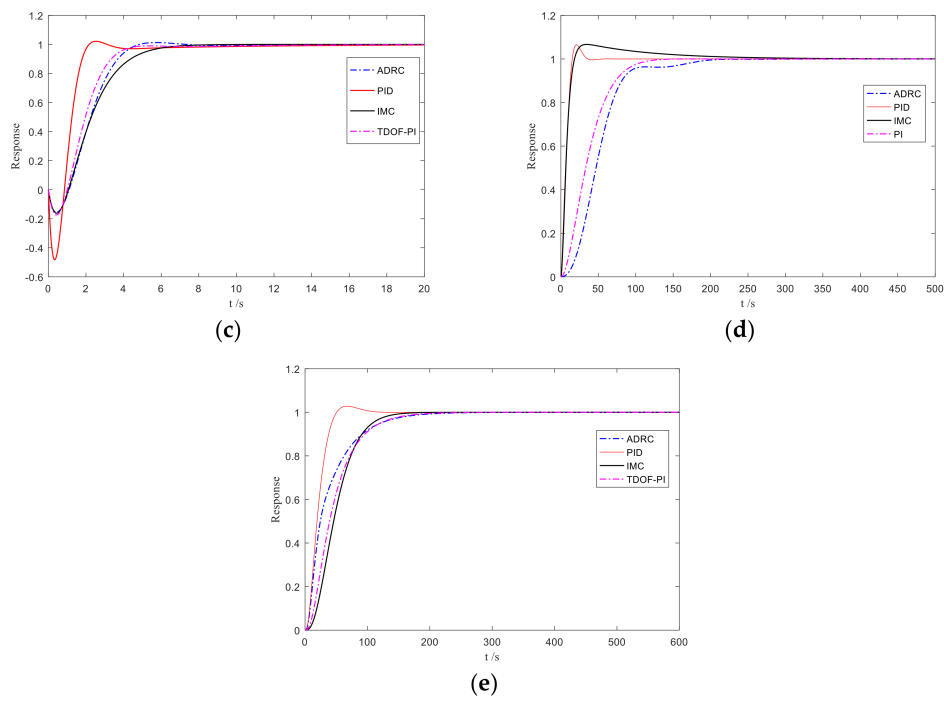


**Figure 3.** The step responses of different nominal plants with different controllers ((a) plant 1; (b) plant 2; (c) plant 3; (d) plant 4; (e) plant 5).

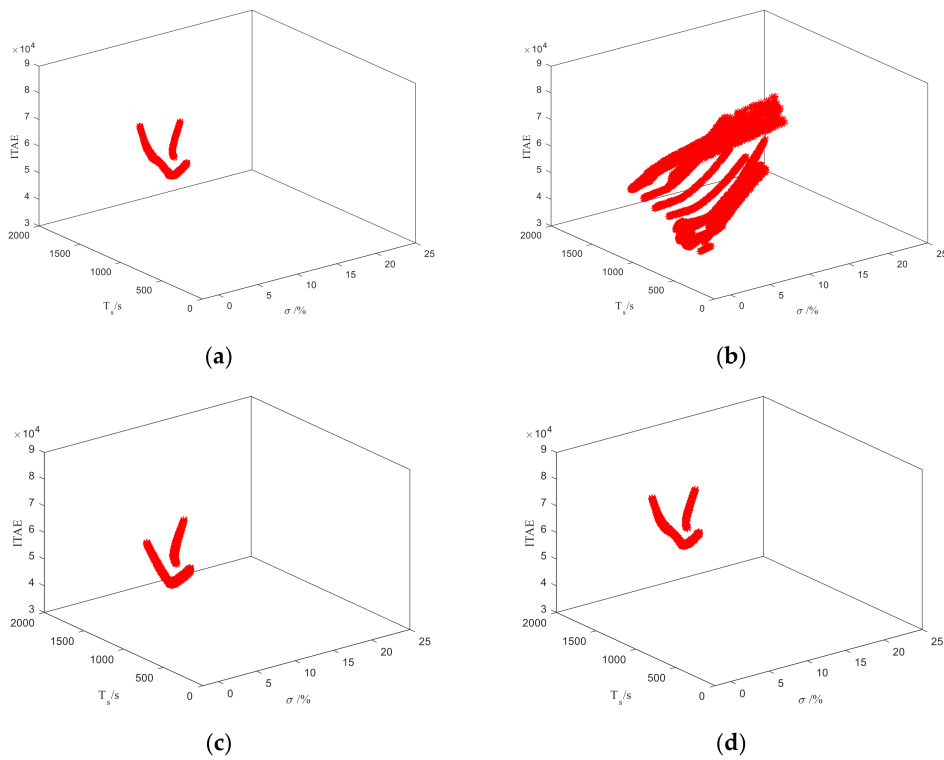


**Figure 4.** Results of Monte Carlo simulation for plant 1 ((a) ADRC; (b) PID; (c) IMC; (d) TDOF-PI). ITAE = Integral of Time and Absolute Error.

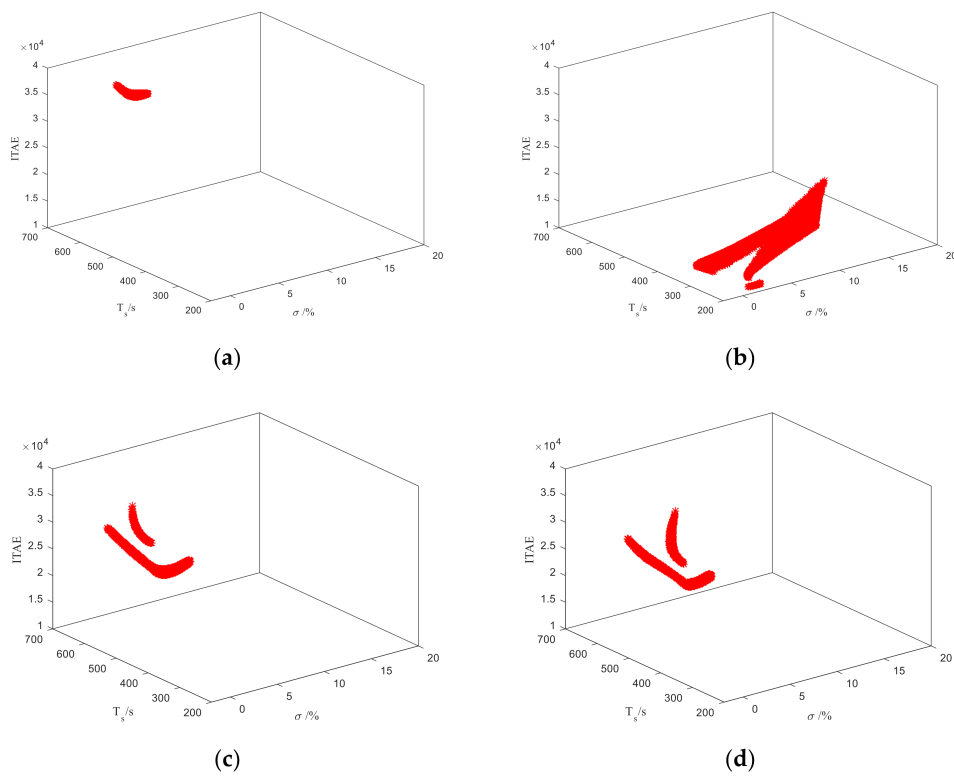


Figure 5. Results of Monte Carlo simulation for plant 2 ((a) ADRC; (b) PID; (c) IMC; (d) TDOF-PI).

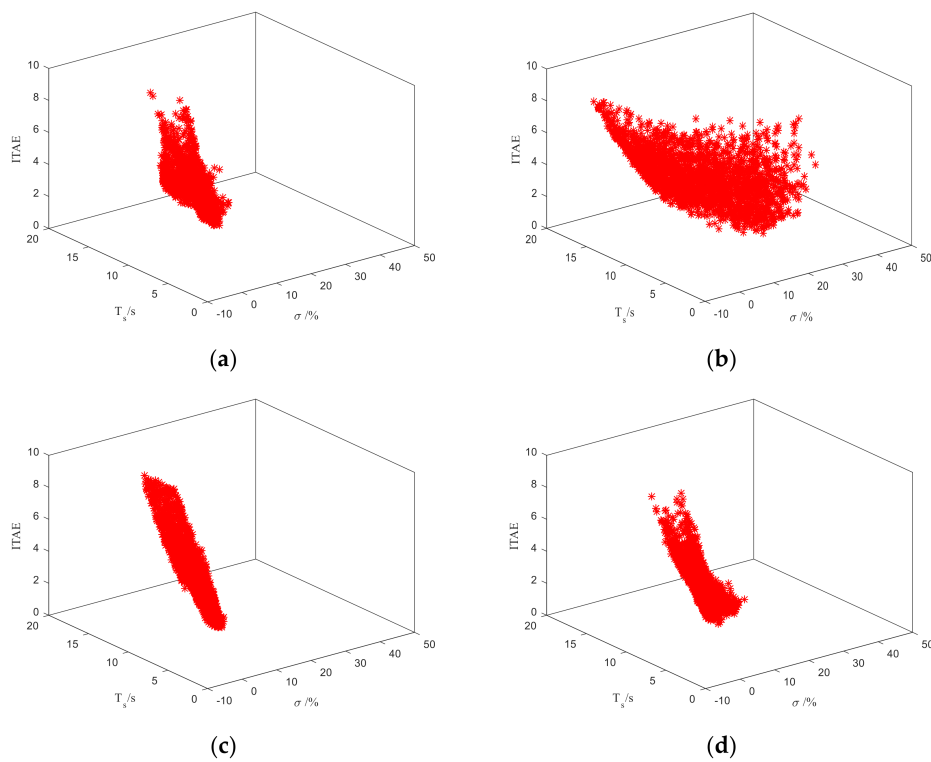


Figure 6. Results of Monte Carlo simulation for plant 3 ((a) ADRC; (b) PID; (c) IMC; (d) TDOF-PI).

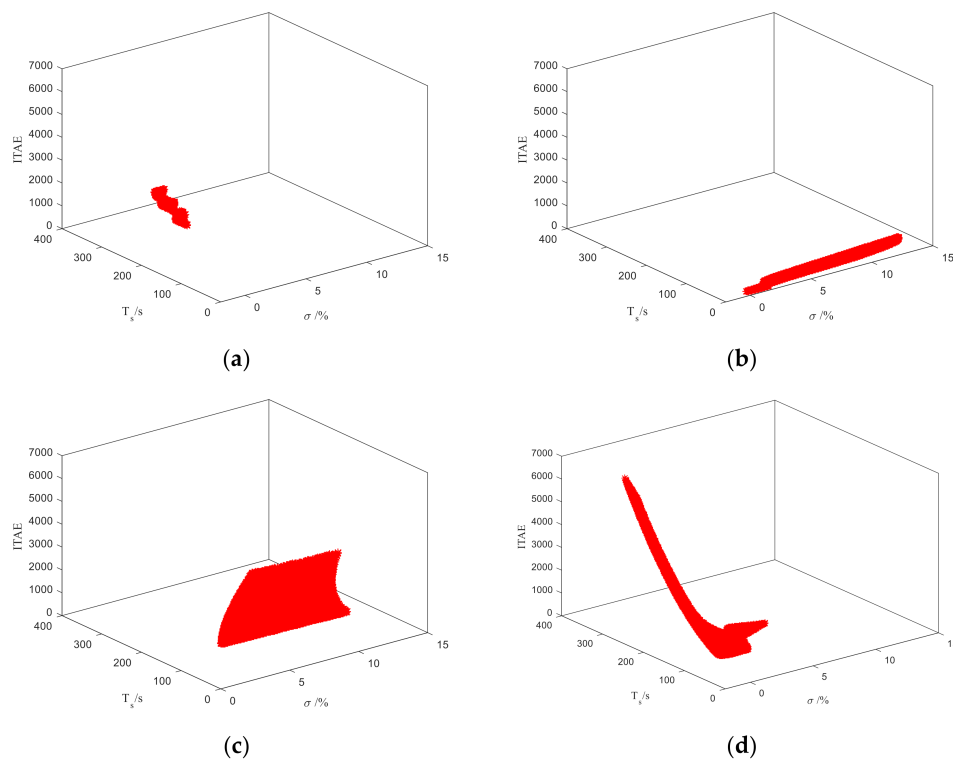


Figure 7. Results of Monte Carlo simulation for plant 4 ((a) ADRC; (b) PID; (c) IMC; (d) PI).

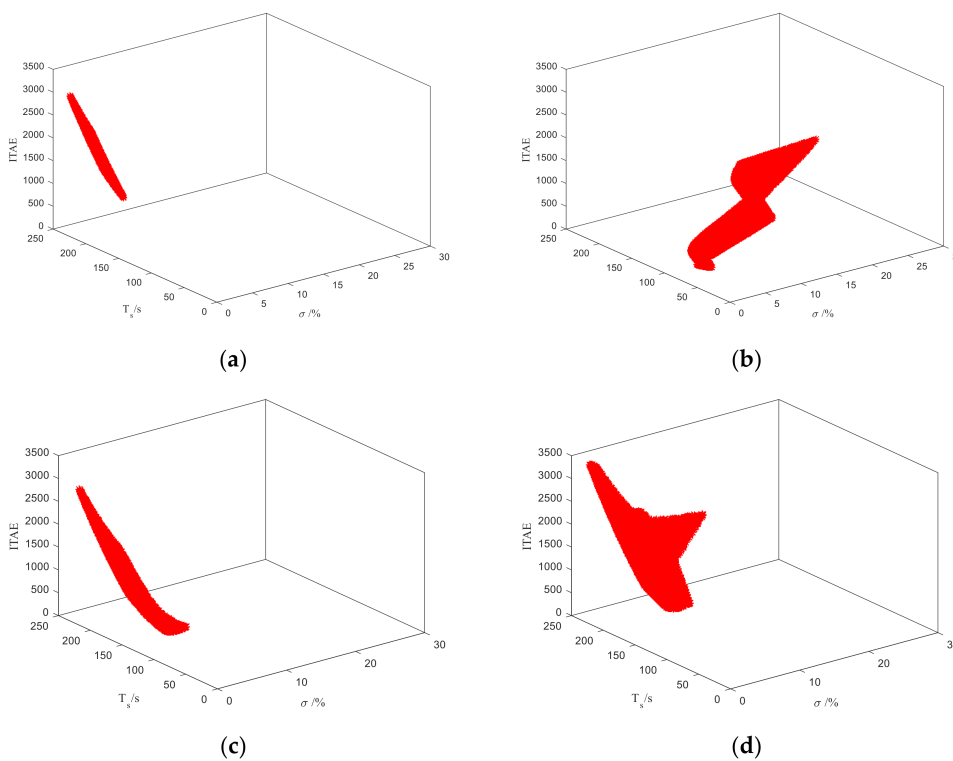


Figure 8. Results of Monte Carlo simulation for plant 5 ((a) ADRC; (b) PID; (c) IMC; (d) TDOF-PI).

From Figure 3, the PID controller has the fastest tracking speed, but it still has the largest overshoot for all plants except plant 4. The ADRC controller, TDOF-PI controller, and IMC controller have similar responses for plant 1, plant 2, plant 3, and plant 5, and they all have small overshoot (less than 2%)

and a similar settling time. Besides this, the IMC controller has the largest overshoot (6.6%) and the overshoot of the PID controller is 6.4% for plant 4, which means that the IMC controller and the PID controller cannot meet the design requirement of the overshoot. What needs to be stressed is that the ADRC controller and the TDOF-PI controller both meet the design requirements for all plants even though the settling time is larger than that of the PID controller. Note that the responses shown in Figure 3 only reflect the control performance of the nominal plants and not all of the plants in the parameter space  $Q$ .

A denser distribution denotes stronger robustness and a smaller value denotes better control performance in Figures 4–8. The value of  $K/N$  listed in Table 4 is the specific value of the estimated value of the probability in Monte Carlo simulation, which means that a larger value denotes stronger robustness and a larger probability to meet the design requirements in the whole parameter space  $Q$ .

From Figure 4, we can know that the ADRC controller in Figure 4a, the TDOF-PI controller in Figure 4d, and the IMC controller in Figure 4c have a denser distribution than the PID controller in Figure 4b for plant 1, which means that the PID controller has the worst robustness, and the value of the PID controller in Table 4 also certifies this. Besides this, the ADRC controller, the TDOF-PI controller, and the IMC controller have a similar distribution, which means that they have a similar robustness, while the value in Table 4 tells that the ADRC controller has the largest probability to meet the design requirements in the whole parameter space  $Q$ .

The ADRC controller in Figure 5a has the densest distribution compared to the PID controller, the TDOF-PI controller, and the IMC controller even though the value of the ITAE index of the ADRC controller is the largest. The value of  $K/N$  of the ADRC controller for plant 2 is larger than 0.999 and it can ensure a large probability to meet the design requirements in the whole parameter space.

The value of  $K/N$  of the ADRC controller for plant 3 is the largest from Table 4, and this means that the ADRC controller has the strongest robustness. Besides this, the distribution of the PID controller is the sparsest in Figure 6b. Note that plant 3 has Right Half Plane (RHP) zero and this is why the value of  $K/N$  of the ADRC controller is smaller than that for other plants.

The ADRC controller in Figure 7a has the densest distribution compared to the PID controller in Figure 7b, the TDOF-PI controller in Figure 7c, and the IMC controller in Figure 7d, which means that the ADRC controller for plant 4 has the the largest probability to meet the design requirements in the whole parameter space  $Q$ , and the value of  $K/N$  of the ADRC controller for plant 4 in Table 4 is also certifies it.

From Figure 8, we can know that the ADRC controller in Figure 8a has the densest distribution compared to the PID controller, the TDOF-PI controller, and the IMC controller, and the value of  $K/N$  of the ADRC controller in Table 4 is 1, which means that ADRC can ensure that uncertain plants in the whole parameter space  $Q$  for plant 5 all meet the design requirements according to the Massart Inequality.

Summarizing the different controllers for the above five examples, ADRC based on the PR index has the largest estimated value of the probability for all plants except plant 2 and has the most possibility to obtain the design requirements throughout the whole parameter space. Note that ADRC based on the PR index still ensures a high probability (0.991) to meet the design requirements throughout the whole parameter space for plant 2. These illustrative simulations demonstrate the effectiveness of the proposed tuning method to enhance the ability of handling the uncertainties for a controller and they offer good support for the application of the proposed method to a boiler unit. A field application to the secondary air regulation of a boiler unit is described below.

## 4. A Field Application to the Secondary Air Regulation of a Boiler Unit

### 4.1. The Process Description

An air control system is an important subsystem for a boiler unit. An air control system can be depicted as in Figure 9. It mainly contains a primary air system, a secondary air system, a fluidizing air

system, and an induced draft system. Secondary air enters into the furnace after passing through the air preheater under the force of secondary air fans as shown in the green part of Figure 9. The function of the secondary air system is to adjust the combustion and the temperature distribution by adjusting the frequency of secondary air fans. Secondary air flow is important for the economy and environmental protection of a boiler unit, which influences the combustion efficiency and generation of nitrogen oxides ( $NO_x$ ) in the combustion [37,38]. The change of the amount of primary air and the bed temperature leads to a wide variety of dynamic characteristics of a secondary air system. What is worse, to integrate more renewable energy into the power grid, the frequent change of load output of a boiler unit results in this being worse.

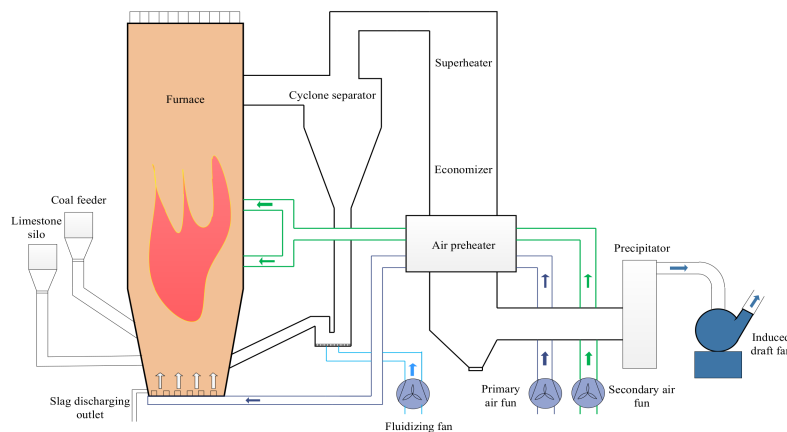


**Figure 9.** Air control system for a boiler unit.

To obtain the expected control performance in a wide range of operating conditions, ADRC controller tuning based on PR is applied to the secondary air regulation shown in Figure 9. This comparative field application was done in Tongda Power Plant, which is a 300 MW Circulating Fluidized Bed (CFB) subcritical unit located in Shanxi Province in China. Some key parameters of the unit in design condition are listed as follows: the output power is 300 MW, the bed temperature is 900 °C, the superheated steam temperature is 541 °C, and the pressure of the main steam is 17.5 MPa. Control logics of ADRC were configured in a DCS platform, which was produced by Zheda Zhongkong Co., Ltd., Hangzhou, China. Besides this, the total amount of the secondary air is about 84.6 m<sup>3</sup>/s in Boiler Maximum Continue Rate (BMCR) condition and the rate of the fans is 1242.5 r/min in BMCR condition.

To obtain a simple model of the secondary air system, the opening loop test was done and the rough model is identified as Equation (36) with the boiler unit working in the condition of 200 MW, which is the common output for the unit. The control variable is the frequency of secondary air fans, there are two of the same fans in the secondary air system (their frequency donates MV1 and MV2, and the average frequency donates MV), and its unit is a percentage of the maximum (%). The output is the total amount of secondary air, which is expressed as a percentage (PV in Figure 10). The result comparison of the test data and the plant data is shown in Figure 10. It shows that the established model can reflect the real dynamic characteristics well. So, the model in Equation (36) is set as the nominal model to design an ADRC controller in the next subsection.

$$G = \frac{k_1}{(T_1s + 1)^2} e^{-\tau_1 s} = \frac{1.967}{(14s + 1)^2} e^{-6s} \quad (36)$$

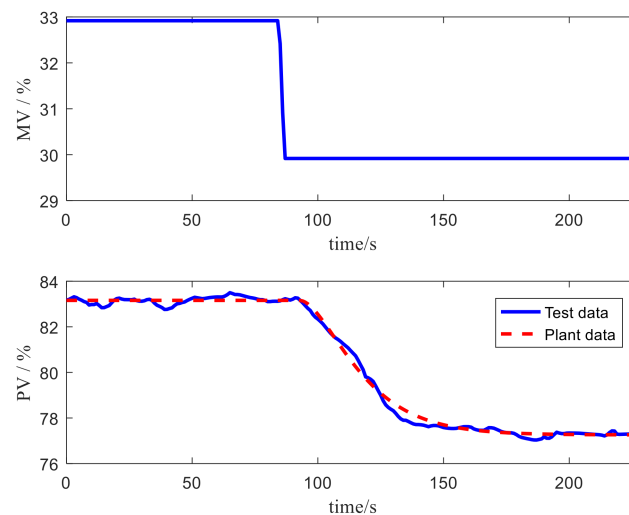


**Figure 10.** Comparison of test data and the model data.

#### 4.2. ADRC Controller Design Based on PR

The ADRC controller based on PR is designed for the nominal model (36), and the parameter perturbation ranges are set as  $k_1 \in [1.5, 2.5]$ ,  $T_1 \in [11, 17]$ , and  $\tau_1 \in [3, 9]$  considering the load range of 50–100%. Design requirements and parameters of Massart Inequality are set as  $T_s < 160s$ ,  $\delta < 5\%$ , and  $\varepsilon = 0.01$ ,  $\sigma = 0.01$ ,  $\alpha = 0.2$ , and  $N = 24494$ , respectively. Parameters of genetic algorithms are the same as those of the simulations in Section 3.  $b_0$  is also fixed as 1 for the nominal model, and the other parameters are obtained as  $\omega_c = 0.2504$ ,  $\omega_o = 0.3458$ , and  $\zeta = 0.3596$  by genetic algorithms.

The step responses of the nominal plant are shown as the black line in Figure 11 and varying plants in the parameter space are shown in Figure 11, and the result of the Monte Carlo simulation is shown in Figure 12. From Figures 11 and 12, we can know that ADRC based on PR can ensure the required control performance and also has a good robustness for the secondary air system working in a wide range. Besides, the value of the PR index  $J$  is 0.9912, which means that the ADRC controller based on the PR index has a large enough probability to meet the design requirements for the secondary air system whose parameters perturb in the perturbation ranges. The simulation based on the identified plant certifies the effectiveness of the proposed method and it gives us great confidence for the following field application.

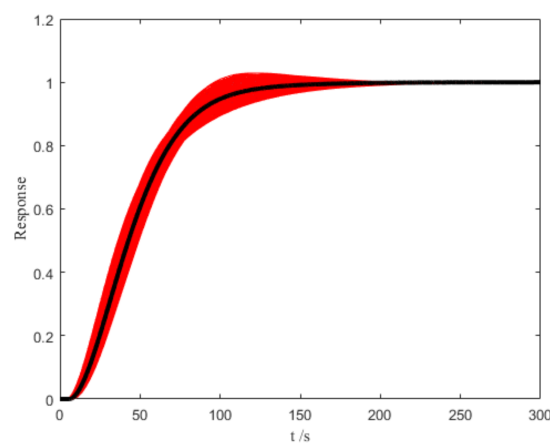


**Figure 11.** The step responses with the nominal plant and varying plants (Black line: the nominal plant, red line: varying plants).

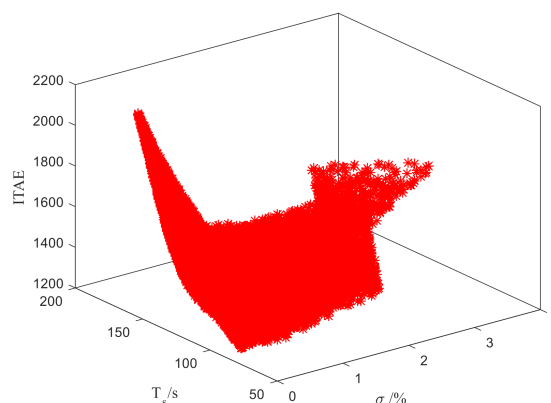


Figure 12. The robustness test by the Monte Carlo simulation.

### 4.3. The Field Application

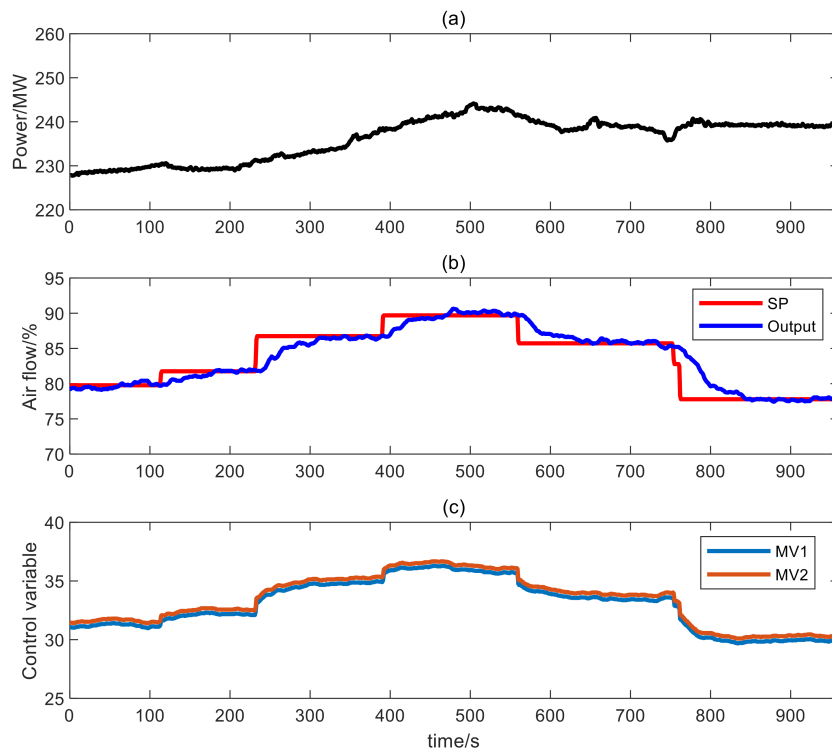
Based on the simulation for the identified plant and some other protective measures done in the DCS platform, the field application of the ADRC controller with the parameters tuned by the proposed method was carried out. Besides this, a similar experiment of a PI controller whose parameters ( $k_p = 1/3, k_i = 1/120$ ) are tuned by experienced engineers was also carried out.

The comparison results of the ADRC and PI controllers are shown in Figures 13 and 14, and the time spans are both 16 min. Figures 13a and 14a show the fluctuation of the unit load during the experiment. Note that the fluctuation range of the ADRC controller is from 228 MW to 245 MW, which is much larger than that of the PI controller from 230 MW to 240 MW. Besides, the settling time and the change amplitude of the secondary air set-point shown in Figures 13b and 14b, respectively, are both listed in Table 5. Obviously, the ADRC controller can track the set-point (SP in Figure 13b) with no static deviation in a short time while the PI controller will need more time to track the set-point (SP in Figure 14b) and sometimes even cannot reach the steady state in the last two set-point changes as shown in Figure 14b. Besides this, the average settling time of the ADRC controller is about 91.2 s, which is much smaller than that of the PI controller (no less than 151 s). Note that the reference signals of the secondary air system in Figures 13b and 14b are different because the load was always changing according to the AGC commands. The control variable of the ADRC controller shown in Figure 13c is smoother than that of the PI controller in Figure 14c, and this is of benefit for the long-time running of the unit.

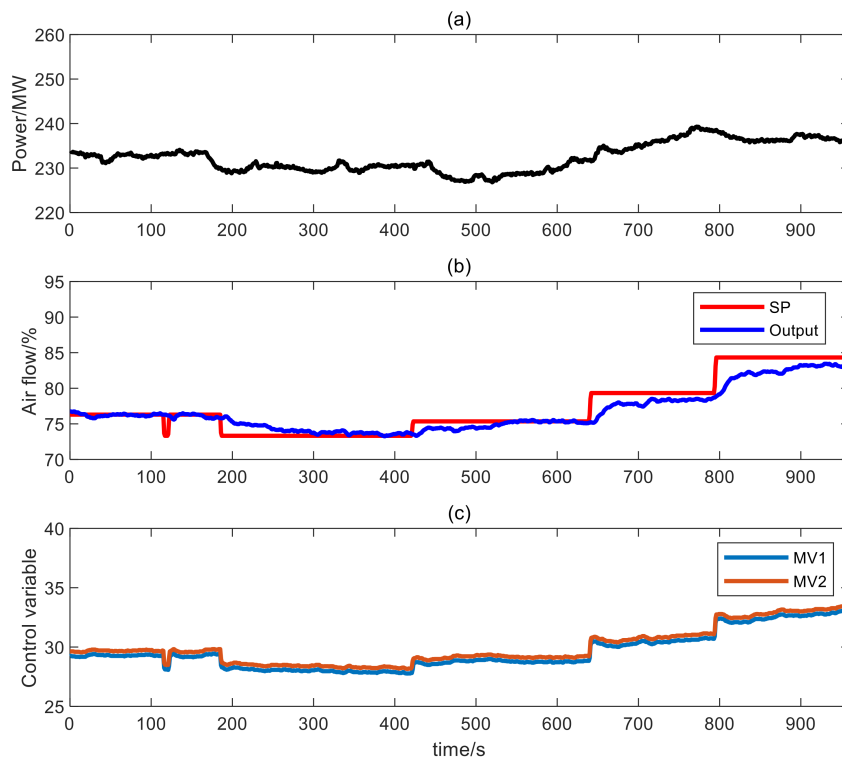
The ability of the ADRC controller based on PR is verified by the comparative experiments, which can obtain expected control performance for the secondary air system working in a wider range of operating conditions. Besides, the load during the experiment is far from 200 MW, which is the load of the opening loop test, and this means that the secondary air system with the ADRC controller can obtain the expected control performance even though the working condition is far from the design condition. Generally, an ADRC controller can play an important role in frequent load regulation, which can facilitate the wide application of sustainable power systems.

Table 5. The settling time of ADRC and PI.

ADRC		PI	
The Change Amplitude	The Settling Time	The Change Amplitude	The Settling Time
$\Delta r = 2$	77 s	$\Delta r = 3$	161 s
$\Delta r = 5$	87 s	$\Delta r = 2$	130 s
$\Delta r = 3$	103 s	$\Delta r = 4$	>164 s
$\Delta r = 4$	95 s	$\Delta r = 5$	>149 s
$\Delta r = 8$	94 s		



**Figure 13.** The field test result of the ADRC controller. SP = set-point. ((a) the power output; (b) the secondary air set-point and output; (c) control variable)



**Figure 14.** The field test result of the PI controller ((a) the power output; (b) the secondary air set-point and output; (c) control variable).

## 5. Conclusions

To achieve a sustainable future for renewable energy and integrate more renewable energy into the power grid, the conventional power plant has to lift its load frequently for a grid balance purpose. This inevitably brings some uncertainties to the power generation side and imposes new challenges for controller design. To improve the boiler control performance in conventional power generation, a data-driven control strategy, namely, ADRC based on PR, is proposed to handle the challenge in this paper. The stability region of the ADRC controller is analysed to provide the search space for the optimization of the PR index, and the design procedure is analysed and summarized. Five illustrative simulations are carried out to demonstrate the effectiveness of the proposed tuning method. With the confidence from the preliminary works, an ADRC controller was applied to the secondary air control of a boiler successfully. The running data shows that the proposed ADRC based on PR can ensure the expected control performance even though it works in a wider range of operating conditions and this depicts a promising future for ADRC controllers in the facilitation of sustainable power systems.

**Acknowledgments:** This work was supported by the National Key Research and Development Program of China under Grant No. 2016YFB0901405, the Natural Science Foundation of Jiangsu Province, China under Grant BK20170686, open funding of the state key lab for power systems, Tsinghua University, the Open Fund of the State Key Laboratory of Clean and Efficient Coal-fired Power Generation and Pollution Control and Coal-based Key Scientific and Technological Projects of Shanxi Province under Grant MD2014-07.

**Author Contributions:** Zhenlong Wu and Donghai Li designed the tuning procedure for ADRC based on probabilistic robustness, the simulations, and wrote this paper. Zhenlong Wu and Ting He designed and performed the field application to the boiler secondary air regulation. Li Sun and Yali Xue has enriched the manuscript in terms of scientific and technical expertise with improving the paper's quality. All authors contributed to bringing the manuscript into its current state.

**Conflicts of Interest:** The authors declare no conflict of interest. The founding sponsors had no role in the design of the study; in the collection, analyses, or interpretation of data; in the writing of the manuscript, and in the decision to publish the results.

## References

1. *International Energy Outlook 2013 Report*; U.S. Energy Information Administration: Washington, DC, USA, 2013.
2. Nguyen, T.T.; Quynh, N.V.; Duong, M.Q.; Van Dai, L. Modified Differential Evolution Algorithm: A Novel Approach to Optimize the Operation of Hydrothermal Power Systems while Considering the Different Constraints and Valve Point Loading Effects. *Energies* **2018**, *11*, 540. [[CrossRef](#)]
3. Son, Y.I.; Kim, I.H.; Choi, D.S.; Shim, H. Robust cascade control of electric motor drives using dual reduced-order PI observer. *IEEE Trans. Ind. Electron.* **2015**, *62*, 3672–3682. [[CrossRef](#)]
4. Hussein, A.A.; Salih, S.S.; Ghasm, Y.G. Implementation of Proportional-Integral-Observer Techniques for Load Frequency Control of Power System. *Procedia Comput. Sci.* **2017**, *109*, 754–762. [[CrossRef](#)]
5. Kobaku, T.; Patwardhan, S.; Agarwal, V. Experimental Evaluation of Internal Model Control Scheme on a DC-DC Boost Converter Exhibiting Non-minimum Phase Behavior. *IEEE Trans. Power Electron.* **2017**, *32*, 8880–8891. [[CrossRef](#)]
6. Zumoffen, D.A.; Braccia, L.; Marchetti, A.G. Economic plant-wide control design with backoff estimations using internal model control. *J. Process Control* **2016**, *40*, 93–105. [[CrossRef](#)]
7. Han, J.Q. From PID to active disturbance rejection control. *IEEE Trans. Ind. Electron.* **2009**, *56*, 900–906. [[CrossRef](#)]
8. Madoński, R.; Herman, P. Survey on methods of increasing the efficiency of extended state disturbance observers. *ISA Trans.* **2015**, *56*, 18–27. [[CrossRef](#)] [[PubMed](#)]
9. Han, J.Q. Active disturbance rejection controller and its applications. *Control Decis.* **1998**, *13*, 19–23.
10. Fu, C.F.; Tan, W. Tuning of linear ADRC with known plant information. *ISA Trans.* **2016**, *65*, 384–393. [[CrossRef](#)] [[PubMed](#)]
11. Gao, Z.Q. Scaling and bandwidth-parameterization based controller tuning. In Proceedings of the American Control Conference, Minneapolis, MN, USA, 14–16 June 2006; pp. 4989–4996.
12. Sariyildiz, E.; Ohnishi, K. Stability and robustness of disturbance-observer-based motion control systems. *IEEE Trans. Ind. Electron.* **2015**, *62*, 414–422. [[CrossRef](#)]

13. Wu, Z.L.; Li, D.H.; Xue, Y.L.; Wang, L.; Wang, J. Active disturbance rejection control for fluidized bed combustor. In Proceedings of the 2016 16th International Conference on Control, Automation and Systems (ICCAS), Gyeongju, Korea, 16–19 October 2016; pp. 1286–1291.
14. Ye, Y.; Yue, Z.; Gu, B. ADRC control of a 6-DOF parallel manipulator for telescope secondary mirror. *J. Instrum.* **2017**, *12*, T03006. [[CrossRef](#)]
15. Sun, L.; Li, D.; Hu, K.; Lee, K.Y.; Pan, F. On tuning and practical implementation of active disturbance rejection controller: A case study from a regenerative heater in a 1000 MW power plant. *Ind. Eng. Chem. Res.* **2016**, *55*, 6686–6695. [[CrossRef](#)]
16. Sun, L.; Hua, Q.; Shen, J.; Xue, Y.; Li, D.; Lee, K.Y. A Combined Voltage Control Strategy for Fuel Cell. *Sustainability* **2017**, *9*, 1517. [[CrossRef](#)]
17. Rahman, M.M.; Chowdhury, A.H.; Hossain, M.A. Improved Load Frequency Control Using a Fast Acting Active Disturbance Rejection Controller. *Energies* **2017**, *10*, 1718. [[CrossRef](#)]
18. Tang, H.; Li, Y. Development and active disturbance rejection control of a compliant micro-/nano-positioning piezo-stage with dual mode. *IEEE Trans. Ind. Electron.* **2014**, *61*, 1475–1492. [[CrossRef](#)]
19. Liu, Y.; Liu, J.; Zhou, S. Linear active disturbance rejection control for pressurized water reactor power. *Ann. Nucl. Energy* **2018**, *111*, 22–30. [[CrossRef](#)]
20. Liu, R.J.; Nie, Z.Y.; Wu, M.; She, J. Robust disturbance rejection for uncertain fractional-order systems. *Appl. Math. Comput.* **2018**, *322*, 79–88. [[CrossRef](#)]
21. Huang, C.E.; Li, D.H.; Xue, Y.L. Active disturbance rejection control for the ALSTOM gasifier benchmark problem. *Control Eng. Pract.* **2013**, *21*, 556–564. [[CrossRef](#)]
22. Zhang, H.; Zhao, S.; Gao, Z.Q. An active disturbance rejection control solution for the two-mass-spring benchmark problem. In Proceedings of the American Control Conference (ACC), Boston, MA, USA, 6–8 July 2016; pp. 1566–1571.
23. Huang, C.; Sira-Ramírez, H. A flatness based active disturbance rejection controller for the four tank benchmark problem. In Proceedings of the American Control Conference (ACC), Chicago, IL, USA, 1–3 July 2015; pp. 4628–4633.
24. Zhao, C.Z.; Li, D.H. Control design for the SISO system with the unknown order and the unknown relative degree. *ISA Trans.* **2014**, *53*, 858–872. [[CrossRef](#)] [[PubMed](#)]
25. Wang, L.J.; Li, Q.; Tong, C.; Yin, Y.; Gao, Z.; Zheng, Q.; Zhang, W. On control design and tuning for first order plus time delay plants with significant uncertainties. In Proceedings of the American Control Conference (ACC), Chicago, IL, USA, 1–3 July 2015; pp. 5276–5281.
26. Tan, W.; Fu, C.F. Linear active disturbance-rejection control: analysis and tuning via IMC. *IEEE Trans. Ind. Electron.* **2016**, *63*, 2350–2359. [[CrossRef](#)]
27. Chen, X.; Zhou, K.; Aravena, J.L. Fast universal algorithms for robustness analysis. In Proceedings of the Decision and Control, Maui, HI, USA, 9–12 December 2003; pp. 1926–1931.
28. Calafiore, G.C.; Dabbene, F.; Tempo, R. Research on probabilistic methods for control system design. *Automatica* **2011**, *47*, 1279–1293. [[CrossRef](#)]
29. Calafiore, G.C. Repetitive scenario design. *IEEE Trans. Autom. Control* **2017**, *62*, 1125–1137. [[CrossRef](#)]
30. Wang, C.F.; Li, D.H.; Li, Z.; Jiang, X. Optimization of controllers for gas turbine based on probabilistic robustness. *J. Eng. Gas Turbines Power* **2009**, *131*, 054502. [[CrossRef](#)]
31. Wu, Z.L.; Xue, Y.L.; Pan, L.; Li, D.; He, T.; Sun, L.; Yang, Y. Active disturbance rejection control based simplified decoupling for two-input-two-output processes. In Proceedings of the Chinese Control Conference (CCC), Dalian, China, 26–28 July 2017.
32. Nandong, J. Heuristic-based multi-scale control procedure of simultaneous multi-loop PID tuning for multivariable processes. *J. Process Control* **2015**, *35*, 101–112. [[CrossRef](#)]
33. Åström, K.J.; Panagopoulos, H.; Hägglund, T. Design of PI controllers based on non-convex optimization. *Automatica* **1998**, *34*, 585–601. [[CrossRef](#)]
34. Wang, C.F.; Li, D.H. Decentralized PID controllers based on probabilistic robustness. *J. Dyn. Syst. Meas. Control* **2011**, *133*, 061015. [[CrossRef](#)]
35. Wang, C.F.; Li, D.H.; Jiang, X.Z. A PID Controller Design Method Based on Probabilistic Robustness. *Proc. CSEE* **2007**, *32*, 020.
36. Ahn, C.W. *Practical Genetic Algorithms*; John Wiley & Sons: Hoboken, NJ, USA, 2006.

37. Kuang, M.; Li, Z.Q.; Ling, Z.Q.; Zeng, X. Improving flow and combustion performance of a large-scale down-fired furnace by shortening secondary-airport area. *Fuel* **2014**, *121*, 232–239. [[CrossRef](#)]
38. Luo, R.; Fu, J.P.; Li, N.; Zhang, Y.; Zhou, Q. Combined control of secondary air flaring angle of burner and air distribution for opposed-firing coal combustion. *Appl. Therm. Eng.* **2015**, *79*, 44–53. [[CrossRef](#)]



© 2018 by the authors. Licensee MDPI, Basel, Switzerland. This article is an open access article distributed under the terms and conditions of the Creative Commons Attribution (CC BY) license (<http://creativecommons.org/licenses/by/4.0/>).